# Electron trapping in noncrystalline remote plasma deposited Hf-aluminate alloys for gate dielectric applications

R. S. Johnson,[a)] J. G. Hong, C. Hinkle, and G. Lucovsky
*Department of Physics, North Carolina State University, Raleigh, North Carolina 27695-8202*

(Received 26 November 2001; accepted 8 April 2002)

The physical and electrical properties of noncrystalline Hf-alumiunate alloys, $(HfO_2)_x(Al_2O_3)_{1-x}$, were investigated. Characterization by Auger electron spectroscopy and Fourier transformation infrared spectroscopy confirm these alloys are homogeneous and pseudobinary in character, displaying increased thermal stability against crystallization with respect to the respective end-member oxides. Capacitance–voltage and current density-voltage data as a function of temperature demonstrate that the Hf $d$ states of these alloys act as localized electron traps, and are at an energy approximately equal to the conduction band offset energy of $HfO_2$ with respect to Si. This work also provides additional insight into a previously reported study of Ta-aluminate alloys with localized electron traps associated with $d$ states of the Ta atoms.  [DOI: 10.1116/1.1481872]

## I. INTRODUCTION

As device dimensions are scaled according to the *1999 International Technology Roadmap for Semiconductors*,[1] the equivalent gate oxide thickness (EOT) must decrease below about 1.5 nm. Scaling of lateral dimensions of Si field effect transistors (FETs) to <100 nm requires replacement of thermally grown $SiO_2$ by deposited dielectrics with higher dielectric constants $k$ than $SiO_2$. The primary motivation for this replacement is based on an assumption that physically thicker films with dielectric constants greater than $SiO_2$, will reduce tunneling, and at the same time produce low defect density interfaces that provide equivalent channel transport for electrons and holes. $Al_2O_3$ and $HfO_2$ have previously been investigated as replacement gate dielectrics for silicon dioxide in complementary metal oxide semiconductor (CMOS) devices.[2,3] This article extends these studies to the aluminate pseudobinary alloy system $(HfO_2)_x(Al_2O_3)_{1-x}$.

It has previously been established that a large amount of intrinsic fixed negative charge, $\sim 6-7\times 10^{12}\,\mathrm{cm}^{-2}$, is present at the internal dielectric interface between $Al_2O_3$ and $SiO_2$.[4,5] Alloying $Al_2O_3$ with a transition metal oxide that has inherent positive interfacial charge such as $HfO_2$ represents a possible way to compensate the negative charge of the $Al_2O_3$ and thereby provide a charge neutral interface that will yield improved channel transport of electrons and holes.

Fourier transformation infrared (FTIR) spectroscopy results in Fig. 1 suggests that Hf atoms substitutionaly replace the six-fold coordinated Al atoms in the $(HfO_2)_x(Al_2O_3)_{1-x}$ alloys and form a homogenous oxide with unique electrical and physical characteristics. This interpretation of the FTIR spectra is consistent with increases in the effective crystallization temperatures of the alloys by at least 100 °C compared with the respective end-member oxides. The crystallization temperatures of Al-rich compositions are increased from 900 °C for $Al_2O_3$ to 1000 °C and those of the Hf-rich compositions are correspondingly increased to 900 °C.

Robertson has calculated the band gaps and band offset energies with respect to Si for $HfO_2$ and $Al_2O_3$,[6] and has obtained values of 1.5 eV for the $HfO_2$–Si band offset and 2.8 eV for the $Al_2O_3$–Si band offset. These assignments are based on crystalline forms of these oxides. Miyazaki has determined a value of 2.08 eV for the offset energy for noncrystalline $Al_2O_3$ using photoemission spectroscopy.[7] The difference between the two values for $Al_2O_3$ is consistent with the differences in coordination between crystalline corundum, $\alpha$-$Al_2O_3$, where the coordination is 6, and noncrystalline $Al_2O_3$, where the ratio of four- to sixfold coordinated Al is 3:1.[8,9]

The lowest lying conduction band states of $Al_2O_3$ are associated with $3s$ and $3p$ states of Al, whereas the lowest lying conduction band states of $HfO_2$ are associated with $5d$ states of Hf.[6] Additionally, these antibonding $d$ states are localized on the Hf atoms,[10] while the Al $3s$ and $3p$ states are significantly more delocalized.

## II. EXPERIMENTAL APPROACH

Thin films of the end-member oxides and their aluminate alloys have been deposited using metal organic bubblers of triethyldialuminum tri-sec-butoxide,[11] and Hafnium $t$-Butoxide. These materials were deposited at a process chamber pressure of 300 mTorr and a 300 °C substrate temperature by remote plasma enhanced chemical vapor deposition (RPECVD).[12]

Metal–oxide–semiconductor junction capacitors were made using a field isolation technique with areas of 50×50 $\mu\mathrm{m}^2$ on 0.06–0.08 $\Omega$ cm boron doped and 0.02–0.05 $\Omega$ cm phosphorous doped $p$- and $n$-type Si substrates. Prior to the aluminum gate contact evaporation, the samples were annealed at temperatures between 800 and 900 °C, which are below the effective composition dependent crystallization temperatures, in an argon ambient for 30 s using an AG Associates minipulse rapid thermal annealer (RTA). It has been shown for silicon dioxide deposited by RPECVD at 300 °C that a RTA is necessary to promote structural and

[a)]Electronic mail: rsj@unity.ncsu.edu

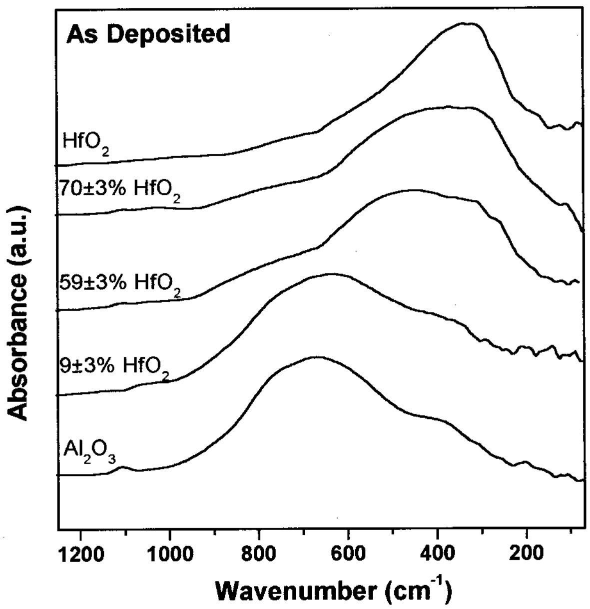


FIG. 1. FTIR spectra for as deposited Hf aluminates and the end-members oxides, $Al_2O_3$ and $HfO_2$. The spectra of the Hf aluminates cannot be obtained by a linear superposition of the two end-member oxide spectra, and thus represent new and unique materials.

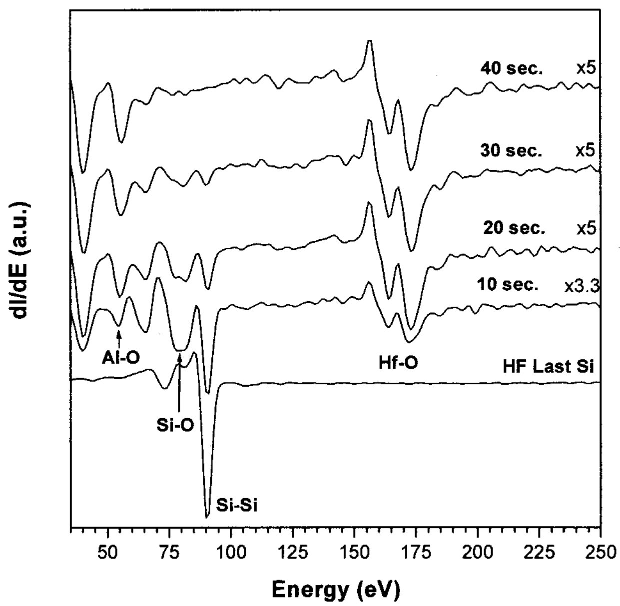


FIG. 2. AES of the initial stages of deposition of Hf aluminates. These results are consistent with previously published $Al_2O_3$ results in Ref. 4, and indicate a thin layer, ~0.6–1.0 nm, of silicon dioxide formation at the silicon interface.

chemical relaxation of the film and its interface with Si and thereby yield electrical performance comparable to devices with thermally grown oxides processed at temperatures between 850 and 1000 °C.[13] After the RTA and prior to the Al gate metal evaporation, a 30 min forming gas anneal with 10% $H_2$ in $N_2$ at 400 °C was preformed. This sequence in which the forming gas anneal was performed prior to metalization was followed to reduce reactions between the Al metal gate and the dielectric films which are known to occur at temperatures as low as 400 °C.[2]

## III. EXPERIMENTAL RESULTS

Interface formation for the alloys was investigated with on-line Auger electron spectroscopy (AES) at the initial stages of film deposition (Fig. 2). The deposition process was interrupted every 10 s, and the sample was transferred to the AES chamber of an ultrahigh vacuum compatible multichamber system where an AES scan was performed. The AES spectra revealed two silicon peaks, one for silicon bonded to silicon, Si–Si, at ~91 eV and another of silicon bonded to oxygen, Si–O, at ~76 eV. The Si–Si peak was present for hydrogen-terminated silicon at the start of the deposition. The 76 eV peak appeared after 10 s along with a decrease in the amplitude of the 91 eV peak. The ratio of these two peak amplitudes is consistent with ~0.6 nm of $SiO_2$ being formed at the interface during the initial stages of deposition. An Al–O peak at 54 eV, and Hf–O peaks at 40, 165, and 173 eV were also observed after the alloy deposition process was initiated. After 40 s the Si peaks were no longer visible, and preceding this the Si–O became increasingly larger in relation to the Si–Si peak. The evolutions of the Si–O and Si–Si peaks are consistent with an increasingly thick overlayer of $Al_2O_3$ causing the deeper-lying layers to be attenuated. Results from previously reported $Al_2O_3$ studies indicate that this $SiO_2$ layer remains relatively thin, 0.6 to 1.0 nm, and is not increased for increasing deposition times, or during postdeposition annealing.[4]

Capacitance–voltage ($C-V$) data, displayed in Figs. 3 and 4 was obtained at 1 MHz for the devices at room temperature, and is shown for the two end-member oxides, a 38% $HfO_2$ Hf-aluminate device on *p*-type Si, and a 48% $HfO_2$ Hf-aluminate device on *n*-type Si. The alloy devices

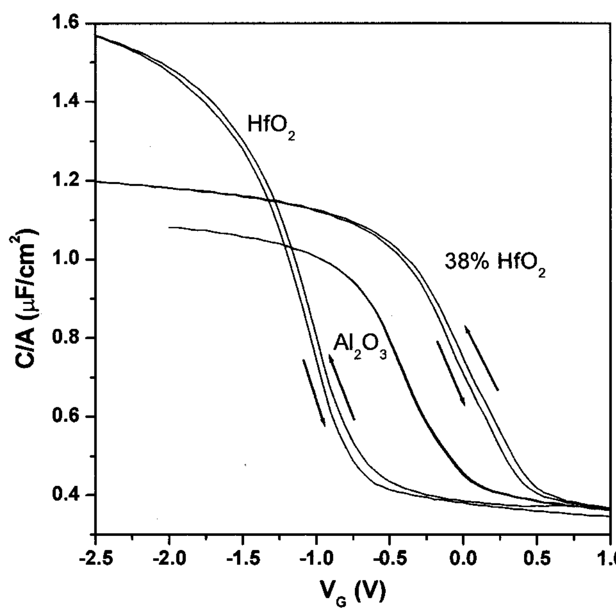


FIG. 3. $C-V$ plots for $Al_2O_3$, $HfO_2$, and 38% $HfO_2$ Hf aluminate on *p*-type silicon substrates with aluminum gates.

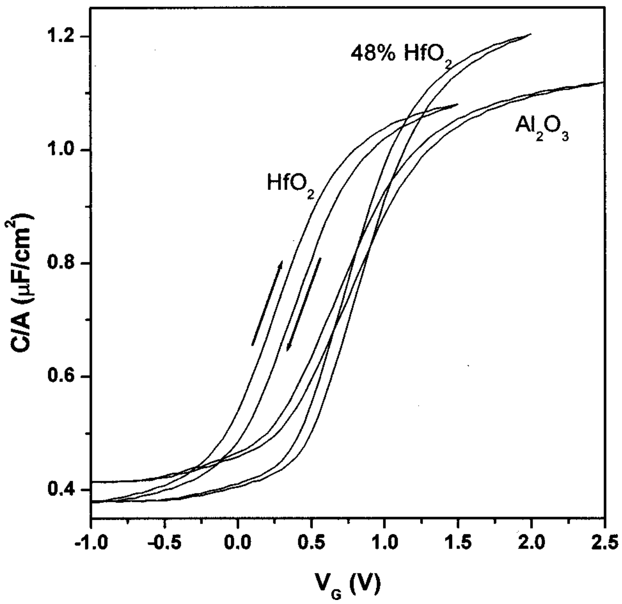


FIG. 4. $C-V$ plots for $Al_2O_3$, $HfO_2$, and 38% $HfO_2$ Hf aluminate on *n*-type silicon substrates with aluminum gates.

display flat-band shifts to more positive voltages with respect the end-member oxides. These positive increases in flat-band voltage are attributed to a negative charge at the Si interface, or within the bulk oxide.[14] The dependence of flat-band voltage on thickness has been used to determine the location of this charge in $Al_2O_3$ dielectrics.[4] For $Al_2O_3$ devices there is a linear dependence on thickness indicating that the charge is located at the interface between the $Al_2O_3$ film and the interfacial $SiO_2$ layer.[14] This assignment is also supported by the temperature dependent $C-V$ and current–voltage ($J-V$) traces, where the absence of significant hysteresis indicates that the dominant contribution to the positive flat-band voltage shift is due to fixed, and not trapped charge.

The flat-band dependence has not been investigated for the alloys, but the shift to positive values is significantly larger than for the respective end-member oxides, and additionally includes significant hysteresis. This is consistent with a significantly larger negative charge due to trapping of electrons. The direction of the hysterisis is also consistent with electron trapping in the $Al_2O_3$ film in the immediate vicinity of the interface.[15]

Figure 5 shows the temperature dependence of $C-V$ and $J-V$ for the 38% Hf-aluminate device on *p*-type Si. The $C-V$ hysteresis was found to increase for temperatures above 200 °C. From 25 to 200 °C the flat-band voltage increases slightly, and above these temperatures the flat band is essentially constant for the positive to negative gate voltage sweeps. Figures 6(a) and 6(b) are the same plots for 48% Hf-aluminate device on *n*-type Si. There is no significant change in the flat-band voltage or hysteresis until a temperature of 250 °C is reached.

For the $J-V$ temperature dependence in Figs. 5(b) and 6(b), the *x* axis is plotted with a *Frenkle–Poole type scale* as a function of the square root of the electric field. Figure 7 displays $J$ vs $1/T$ at a fixed value of the electric field across

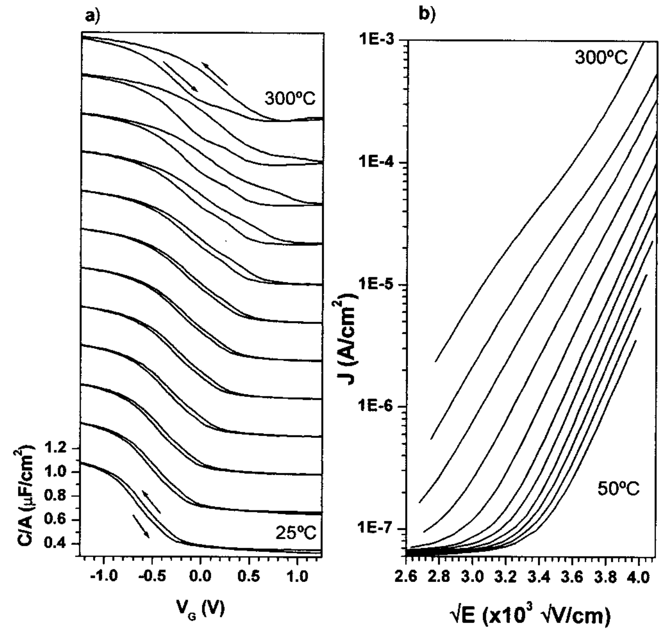


FIG. 5. Temperature dependence of $C-V$ and $J-V$ for 38% $HfO_2$ Hf aluminate on *p*-type silicon substrates with aluminum gates.

the oxide for devices with both *p*-type Si and *n*-type Si substrates.

## IV. DISCUSSION

Shifts in flat-band voltage are generally accepted to be due to either (i) fixed charge, $Q_f$, (ii) mobile charge, $Q_m$, (iii) oxide trapped charge, $Q_{ot}$, or (iv) interface trapped charge, $Q_{it}$, sometimes called $D_{it}$.[15] Hysteresis in $C-V$

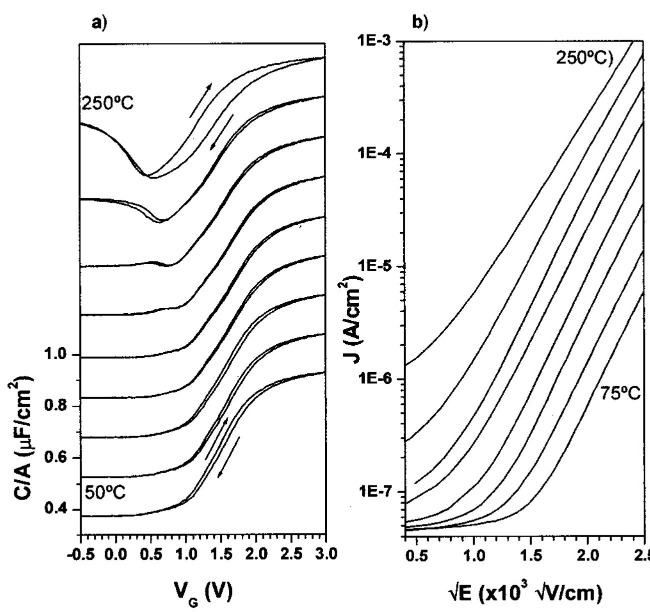


FIG. 6. Temperature dependence of $C-V$ and $J-V$ for 48% $HfO_2$ Hf aluminate on *n*-type silicon substrates with aluminum gates.

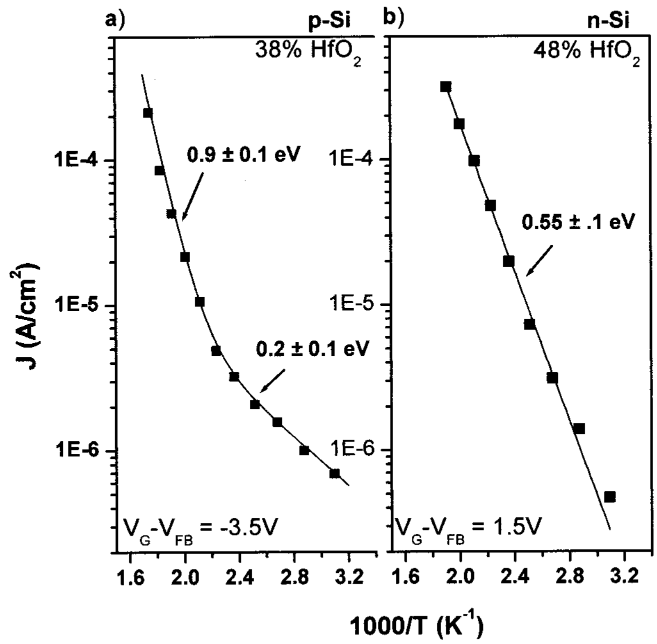


FIG. 7. $J$ vs $1/T$ for both 38% and 48% $HfO_2$ Hf aluminates on $p$- and $n$-type silicon substrates, respectively. Activation energies from exponential fits are included.

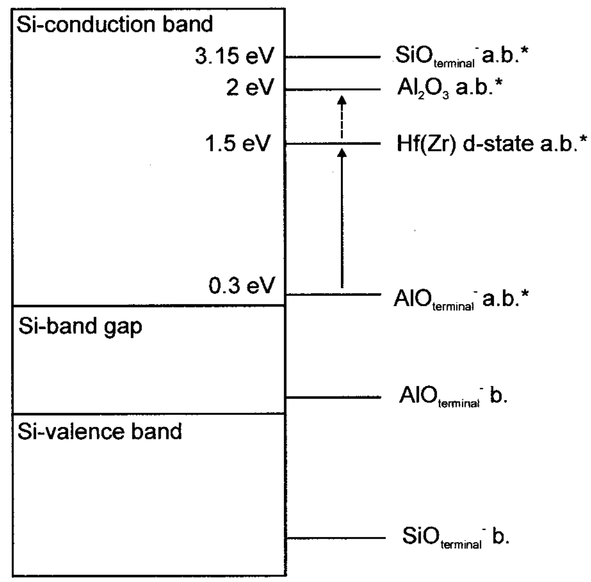


FIG. 8. Localized bonding $b$ and antibonding $ab$, states in Hf aluminates. The left-hand side indicates the conduction and valence bands of the silicon substrate. On the right-hand side are the proposed localized defect states, and bands for the aluminate alloys. The arrows indicate the transitions obtained through the analysis of temperature dependent $C-V$ and $J-V$ measurements. The dashed arrow is for a predicted high temperature transition from the localized Hf $d$ state (not observed) to the aluminum oxide matrix extended conduction band states.

measurements is normally attributed (i) to charge trapping in the oxide or at the interface, (ii) mobile ion charge, or (iii) remnant polarization as in ferroelectrics.[15]

For the entire temperature range investigated the direction of hysteresis is consistent with charge trapping. Mobile charge is generally attributed to positive ion impurities such as $Na^+$, $Li^+$, and $K^+$ and gives a hysteresis loop in the opposite sense to what is displayed in Figs. 5(b) and 6(b).[14] Neither organic source contains these metals either as molecular constituents or as impurities. In addition, we have followed standard $SiO_2$ processing guidelines that in our previous results have indicated no evidence for mobile charge in deposited $SiO_2$ dielectrics. Finally, there is no evidence for these impurities in the respective end-member oxides.

The temperature dependence of the conduction through an insulating film can be derived from two mechanisms: (i) carrier excitation, such as trap release, and (ii) transport.[16] Each of these mechanisms can have a temperature dependence described in the form of Eq. (1) where $W$ is an effective activation energy, and $\beta_o$ is an *appropriate* prefactor:

$$\beta_t = \beta_o \exp(-W/kT). \tag{1}$$

A single activation energy has been used to characterize the temperature dependence in each temperature range in Fig. 7. We have not made any attempt to separate the excitation and transport mechanisms because of the assumptions that are required. Instead we analyze the temperature dependent $J-V$ in terms of carrier activation processes alone. This approach assumes that over the range of temperatures explored any contributions to the activation energy from temperature dependent transport processes are small. The activation energies obtained in this way are interpreted using an energy level scheme in Fig. 8 that is consistent with experimentally determined band conduction band offset energies.[6,7] In addition, it includes a new proposal for defect states that are generated by a disruption of the $Al_2O_3$ network bonding component.[6,7,17]

Figure 7(a) can be fit with by two exponential functions with different activation energies. For devices Ta-aluminate dielectrics the two activation energies were associated with the energy of localized Ta antibonding $d$ states relative to the Si conduction band, and the offset energy of the $Al_2O_3$ extended conduction band $s$ states.[18] Unlike the Ta aluminates, the Hf aluminates do not display a decrease in flat-band voltage or a change in hysteresis for the highest temperatures used in this study. For the Ta-aluminates discussed in Ref. 18, the low temperature activation energy of ~0.3 eV was attributed to the filling of Ta $d$ states, and the second energy was attributed to a release from these localized Ta $d$ state traps in extended states of the $Al_2O_3$ host matrix conduction band. The release into transport states produced a decrease in hysteresis initially, and then a reversal in the hysteresis sense, as well as a significant decrease in the flat-band voltage.[18] For Hf aluminates the second activation energy regime level is accompanied with an increase in hysteresis, and an increase in flat-band voltage shift. These two effects are consistent with a two-level trapping system where electrons are not injected into the aluminum oxide matrix conduction band states at the highest measurement temperatures, but rather into a second set of trapping states.

If we assume that the two activation energies for the Hf-aluminate alloy dielectrics correspond to two different trap levels, then the initial energy 0.2 eV is the barrier height for injection into the first trap, and the second 0.9 eV is energy difference between these two trapping states, modified by an appropriate Schottky barrier lowering. To calculate the level of the second trapping state, we add the two activation energies, and also include a Schottky barrier lowering of 0.3 eV, which is appropriate to the high field of $9\times10^6$ V/cm at which this process has been observed. This results in a trap energy relative to the Si conduction band of 1.4 eV, which is very close to the estimated 1.5 eV conduction band offset of the $HfO_2$ antibonding *d* states.[6]

The question of the origin of the first activation energy for Hf aluminates is now addressed. Even though it is approximately the same as the initial trapping state energy reported for the Ta aluminate alloys, it cannot be assigned to an intrinsic antibonding state of the Hf aluminate alloys. Molecular orbital theory calculations are being preformed by our group and collaborators on transition metal silicate and aluminate alloys.[17] These studies are consistent with the bonding of metal atoms in silicate glasses.[19] For the addition of $Hf(Zr)O_2$ into an $SiO_2$ continuous random network, two Si–O bonds are broken and these form four terminal network oxygen atoms with negative charge introducing a silicate bonding feature into the infrared absorption spectrum at 910–20 $cm^{-1}$.[20] Studies of Zr and Hf silicate alloys indicate that the bonding and antibonding states of this terminal, $SiO^{1-}_{terminal}$ group are well removed from the silicon band gap, since they are not active as trapping/defect states.[2]

For the Hf aluminate alloys a similar network disruption will occur for the addition of $HfO_2$ into an $Al_2O_3$ host, simply because of the increased ratio of O to Hf in the $HfO_2$ alloy component relative to the ratio O to Al in $Al_2O_3$. Based on the local bonding of Al atoms in $Al_2O_3$, this alloy oxide insertion will also disrupt the network bonding $AlO^{1-}_{4/2}$ component of the $Al_2O_3$, and generate two terminal $AlO^{1-}_{terminal}$ groups. However, the $AlO^{1-}_{terminal}$ group does not occur naturally in any crystalline material and, therefore, is assumed to be less stable than the $SiO^{1-}_{terminal}$ group, which is a constituent of all silicate glasses in the low alloy.[19] In addition, empirical calculations based on electronegativity models also indicate that it is significantly less stable than the $SiO^{1-}_{terminal}$ group due to a higher ratio of electrons to nuclear charge. This suggests that the bonding and antibonding states of the $AlO^{1-}_{terminal}$ may be in or near the band gap of silicon and, therefore, be active as trapping/defect states. For the Ta aluminates the localized Ta *d* state is low in energy, and may overlap with this network disruption defect state, thereby making it difficult, if not impossible to distinguish between the disruption defect state and the localized Ta *d* state based on an analysis of *J* vs *T* data alone.[6,18] This point is supported by the quantitative differences between low temperature trapping of the Ta and Hf aluminate alloys. The trapping in the Ta aluminate devices is larger, consistent with the trapping state being an intrinsic energy level of the alloy, rather than a defect that results from the alloy formation and network disruption process.

Figure 7(b) presents for similar results for Hf aluminate dilectrics using *n*-type silicon substrates in which electron injection is from the substrate rather than the gate electrode. The temperature range is not as large as with the *p*-type silicon substrates because of a significant increase in leakage current.[4] Here there is only one activation energy present, however, the possibility of a second higher temperature activated trapping process is anticipated by the increase in the hysteresis of the $C-V$ traces at the 250 °C measurement temperature.

A much larger energy barrier for hole injection eliminates the possibility that we are measuring hole traps. The valence band offset energy with respect to silicon as measured by photoemission spectroscopy[7] for $Al_2O_3$ is 3.75 eV, and as calculated for $HfO_2$ (Ref. 6) is 3.4 eV.

## V. CONCLUSIONS

From the temperature dependence of $C-V$ and $J-V$ traces for $Al_2O_3-HfO_2$ alloys, we have concluded that there are two localized electron traps at approximately 0.2–0.3 and 1.4 eV above the Si conduction band edge. The 0.2–0.3 eV traps are assigned to $AlO^{1-}_{terminal}$ bonding groups that derive from a breaking or *rupturing* of the network component of the $Al_2O_3$ host material, and the 1.4 eV traps are assigned to antibonding Hf atom *d* states that form the lowest conduction bands of these alloys.

Thus, in contrast to the Ta-aluminate dielectrics of Ref. 18, the Hf-aluminate dielectrics of this article demonstrate a two level trapping system, where at low temperatures there is a trapping state due to the $AlO^{1-}_{terminal}$ groups, and at higher temperatures, a release from this state into a localized Hf *d* state. In the high temperature region the flat band increases because two states are now each active as traps. At still higher temperatures the electrons could be thermally emitted from the localized Hf *d* states into the aluminum oxide matrix conduction band, resulting in a decrease in flat-band voltage and hysteresis. In the Ta aluminate alloys, two activation energies were reported, one for trapping into Ta *d* states ~0.3 eV above the silicon conduction band edge, and one for release into conducting states of the $Al_2O_3$ host matrix.[18] The release of electrons from the Ta *d* state traps into conducting states of the $Al_2O_3$ matrix is accompanied by a decrease and reversal in hysteresis, and a decrease in the flat-band voltage shift.

Recent experiments performed in our laboratory have used x-ray absorption spectroscopy to study Zr and Ta antibonding *d* states in $ZrO_2-SiO_2$[21] and $Ta_2O_5-Al_2O_3$ alloys[22] with essentially the same result. Zr and Ta introduce localized *d* states whose energies with respect to deep core states are independent of the alloy compositions and the state of crystallization. The lowest localized *d* states do not mix in any significant way with the extended *s*-like conduction band states of the $SiO_2$ of $Al_2O_3$ alloys. The absence of mixing is consistent with a band picture in which aluminum oxide acts as the bulk transport matrix, and the localized trapping centers are distributed throughout the bulk and have energies with respect to the $Al_2O_3$ and Si conduction bands, which are essentially independent of the alloy compositions.

## ACKNOWLEDGMENTS

This work is supported by the Office of Naval Research, ONR, the Air Force Office of Scientific Research, AFOSR, the Semiconductor Research Corporation, SRC, and the SEMATECH/SRC Front End Processes Center. We acknowledge helpful discussions with Yu Zhang and Jerry Whitten of North Carolina State University, and T. P. Ma of Yale University.

Presented at the IUVSTA 15th International Vacuum Congress and the AVS 48th International Symposium, and the 11th International Conference on Solid Surfaces, San Francisco, CA, 28 October–2 November 2001.

[1] *Semiconductor Industry Association, International Technology Roadmap for Semiconductors*: 1999 ed. (http://public.itrs.net).
[2] L.-A. Ragnarsson, E. Aderstedt, and P. Lundgren, Mater. Res. Soc. Symp. Proc. **367**, 451 (1999).
[3] G. D. Wilk, R. M. Wallace, and J. M. Anthony, J. Appl. Phys. **89**, 5243 (2001).
[4] R. S. Johnson, G. Lucovsky, and I. Baumvol, J. Vac. Sci. Technol. A **19**, 1353 (2001).
[5] G. Lucovsky, J. C. Phillips, and M. F. Thorpe, in *Characterization and Metrology for USLI Technology 2000*, edited by P. G. Seiber, A. C. Diebold, T. J. Shaffner, R. McDonald, W. M. Bullis, P. J. Smith, and E. M. Secula, AIP Conf. Proc. No. 550 (AIP, Melville, NY, 2000).
[6] J. Robertson, J. Vac. Sci. Technol. B **18**, 1785 (2000).
[7] S. Miyazaki and M. Hirose, in *Characterization and Metrology for USLI Technology 2000*, edited by D. G. Seiber, A. C. Diebold, T. J. Shaffner, R. McDonald, W. M. Bullis, P. J. Smith, and E. M. Secula, AIP Conf. Proc. No. 550 (AIP, Melville, NY, 2001).
[8] G. Lucovsky, G. A. Rozaj-Brvar, and R. F. Davis, in *The Structure of Non-Crystalline Materials 1982*, edited by P. H. Gaskell, J. M. Parker, and E. A. Davis (Taylor and Francis, London, 1983), p. 193.
[9] G. B. Rayner, H. Niimi, R. Johnson, R. Therrien, G. Lucovsky, and F. L. Galeener, in *Characterization and Metrology for USLI Technology 2000*, edited by D. G. Seiber, A. C. Diebold, T. J. Shaffner, R. McDonald, W. M. Bullis, P. J. Smith, and E. M. Secula, AIP Conf. Proc. No. 550 (AIP, Melville, NY, 2001).
[10] G. Lucovsky, J. L. Whitten, and Y. Zhang, Microelectron. Eng. **59**, 329 (2001).
[11] R. G. Gordon, K. Kramer, and X. Liu, Mater. Res. Soc. Symp. Proc. **446**, 383 (1997).
[12] T. Yasuda, Y. Ma, S. Habermehl, and G. Lucovsky, J. Vac. Sci. Technol. B **10**, 1844 (1992).
[13] B. J. Hinds, F. Wang, D. M. Wolfe, C. L. Hinkle, and G. Lucovsky, J. Vac. Sci. Technol. B **16**, 2171 (1998).
[14] E. H. Nicollian and J. R. Brews, *MOS (Metal Oxide Semiconductor) Physics and Technology* (Wiley, New York, 1982).
[15] D. K. Schroder, *Semiconductor Material and Device Characterization*, 2nd ed. (Wiley, New York, 1998).
[16] W. C. Johnson, Technical Report No. 7, Princeton University, 1979.
[17] Y. Zhang, G. Lucovsky, and J. Whitten (unpublished).
[18] R. S. Johnson, J. G. Hong, and G. Lucovsky, J. Vac. Sci. Technol. B **19**, 1606 (2001).
[19] R. Zallen, *The Physics of Amorphous Solids* (Wiley, New York, 1983).
[20] G. Lucovsky and G. B. Rayner, Appl. Phys. Lett. **77**, 2912 (2000).
[21] G. Lucovsky, G. B. Rayner, Jr., G. Appel, R. S. Johnson, Y. Zhang, D. E. Sayers, H. Ade, and J. L. Whitten, Appl. Phys. Lett. **79**, 1775 (2001).
[22] G. Appel (unpublished).